Microelectronic Engineering 117 (2014) 57–66

Contents lists available at ScienceDirect

Microelectronic Engineering

journal homepage: www.elsevier.com/locate/mee

Methods of simulating thin film deposition using spray pyrolysis techniques

Lado Filipovic [a,*], Siegfried Selberherr [a], Giorgio C. Mutinati [b], Elise Brunet [b], Stephan Steinhauer [b], Anton Köck [b], Jordi Teva [c], Jochen Kraft [c], Jörg Siegert [c], Franz Schrank [c]

[a] Institute for Microelectronics, TU Wien, Gußhausstraße 27–29/E360, A-1040 Wien, Austria
[b] Molecular Diagnostics, Health & Environment, AIT GmbH, Donau-City-Straße 1, A-1220 Wien, Austria
[c] ams AG, Tobelbaderstrasse 30, A-8141 Unterpremstätten, Austria

ARTICLE INFO

Article history:
Received 19 April 2013
Accepted 13 December 2013
Available online 25 December 2013

Keywords:
Spray pyrolysis deposition
Tin oxide film
Topography simulation
Level Set
Smart gas sensors

ABSTRACT

Integration of thin tin oxide film formation into CMOS technology is a fundamental step to realize sensitive smart gas sensor devices. Spray pyrolysis is a deposition technique which has the potential to fulfil this requirement. A model for spray pyrolysis deposition is developed and implemented within a Level Set framework. Two models for the topography modification due to spray pyrolysis deposition are presented, with an electric and a pressure atomizing nozzle. The resulting film growth is modeled as a layer by layer deposition of the individual droplets which reach the wafer surface or as a CVD-like process, depending on whether the droplets form a vapor near the interface or if they deposit a film only after surface collision.

1. Introduction

Gas sensors are of importance for many applications ranging from air quality monitoring indoors and outdoors to personal safety systems. Different variants of metal oxide based gas sensors, which rely on changes of the electrical conductance due to the interaction with the surrounding gas, have been developed. However, today's gas sensors are bulky devices, which are primarily dedicated to industrial applications. Since they are not integrated in CMOS technology, they cannot fulfil requirements for smart gas sensor applications in consumer electronics.

1.1. Tin oxide based gas sensors

A powerful strategy to improve sensor performance is the implementation of very thin nanocrystalline films, which have a high surface to volume ratio and thus a strong interaction with the surrounding gases. SnO_2 has been the most prominent sensing material and a variety of gas sensor devices based on SnO_2 thin films has been realized so far [1,2]. Spray pyrolysis is a powerful technology for the fabrication of nanocrystalline SnO_2 films for gas sensing applications [3–5]. Spray pyrolysis is a well-known method for the deposition of a wide variety of thin films and has been used for decades in the glass industry [6] and in solar cell production [7]. This technique requires no vacuum, provides high flexibility in terms of material composition, is suitable for fabrication of thin films on full wafer-size, and can be implemented with CMOS technology [8]. Spray pyrolysis is thus a very cost efficient technology, which is a major issue for the development of smart CMOS based gas sensor devices. In order to optimize this technology for the heterogeneous integration of gas sensing layers with CMOS fabricated micro-hotplate chips [9] on a wafer scale, full understanding of the spray pyrolysis deposition process by modeling is an important issue.

1.2. Level Set method

The presented simulations and models function fully within the process simulator presented in [10]. The Level Set method is utilized in order to describe the top surface of a semiconductor wafer as well as the interfaces between different materials. The Level Set method describes a movable surface $\mathcal{S}(t)$ as the zero Level Set of a continuous function $\Phi(\vec{x},t)$ defined on the entire simulation domain,

$$\mathcal{S}t = \{\vec{x} : \Phi(\vec{x},t) = 0\}. \tag{1}$$

The continuous function $\Phi(\vec{x},t)$ is obtained using a signed distance transform

$$\Phi(\vec{x},t=0) := \begin{cases} -\min\limits_{\vec{x}'\in\mathcal{S}(t=0)} \|\vec{x}-\vec{x}'\| & \text{if } \vec{x}\in\mathcal{M}(t=0) \\ +\min\limits_{\vec{x}'\in\mathcal{S}(t=0)} \|\vec{x}-\vec{x}'\| & \text{else,} \end{cases} \tag{2}$$

* Corresponding author. Tel.: +43 1 58801 36036; fax: +43 1 58801 36099.
E-mail address: filipovic@iue.tuwien.ac.at (L. Filipovic).

0167-9317/$ - see front matter © 2013 Elsevier B.V. All rights reserved.
http://dx.doi.org/10.1016/j.mee.2013.12.025

where $\mathcal{M}$ is the material described by the Level Set surface $\Phi(\vec{x}, t = 0)$. The implicitly defined surface $\mathcal{S}(t)$ describes a surface evolution, driven by a scalar velocity $V(\vec{x})$, using the Level Set equation

$$\frac{\partial \Phi}{\partial t} + V(\vec{x})\|\nabla \Phi\| = 0. \tag{3}$$

In order to find the location of the evolved surface, the velocity field $V(\vec{x})$, which is a calculated scalar value, must be found. The Level Set equation belongs to the class of Hamilton–Jacobi equations given by

$$\frac{\partial \Phi}{\partial t} + H(\vec{x}, \nabla\Phi, t) = 0 \text{ for } H(\vec{x}, \nabla\Phi, t) = V(\vec{x})\|\nabla\Phi\|, \tag{4}$$

where H denotes the Hamiltonian. The Level Set equation can then be solved using finite difference schemes such as the Euler method [11], the Upwind scheme, based on the Engquist–Osher scheme [12], or the Lax–Friedrichs Scheme for non-convex Hamiltonians [13].

1.3. Spray pyrolysis deposition

During the last several decades, coating technologies have garnered considerable attention, mainly due to their functional advantages over bulk materials, processing flexibility, and cost considerations [14]. Thin film coatings can be deposited using physical methods or chemical methods. Spray pyrolysis is a technique which uses a liquid source for thin film coating as given in Fig. 1, where CVD and Atomic Layer Epitaxy (ALE) are the gas processes.

Although a liquid source is used, many studies suggest that it is the evaporated liquid near the wafer surface that causes the thin film deposition [15]. This work examines the difference between physical and chemical depositions during spray pyrolysis. The first introduction of the spray pyrolysis technique by Chamberlin and Skarman [16] in 1966 was for the growth of CdS thin films for solar cell applications. Since then, the process has been investigated with various materials, such as SnO_x [17], In_2O_3 [18], indium tin oxide (ITO) [19], PbO [20], ZnO [21], ZrO_2 [22], YSZ [15] and others [23]. The main advantages of spray pyrolysis over other similar techniques are:

- No requirement of vacuum.
- Substrates with complex geometries can be coated.
- Uniform and high quality coatings.
- Implementation as post-CMOS backend process.
- Cost effectiveness.

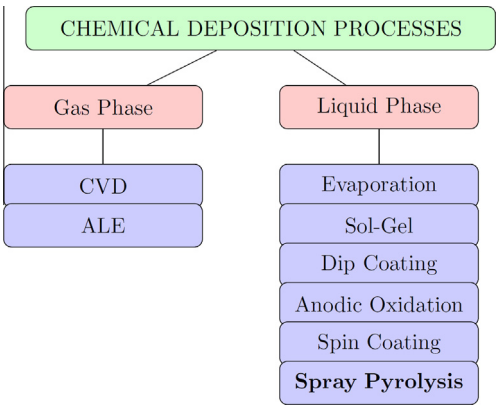

Fig. 1. Summary of chemical thin film deposition technologies.

The spray pyrolysis process is used for the deposition of a transparent layer on glass [24], the deposition of a SnO_2 layer for gas sensor applications [17], the deposition of a YSZ layer for solar cell applications [15], anodes for lithium-ion batteries [25], and optoelectronic devices [26].

The general simplified scheme for spray pyrolysis deposition is shown in Fig. 2, where three processing steps can be viewed and analyzed:

1. Atomization of the precursor solution.
2. Aerosol transport of the droplet.
3. Decomposition of the precursor to initiate film growth

These three steps are individually addressed in the sections to follow.

2. Process sequence during deposition

2.1. Precursor atomization

The atomization procedure is the first step in the spray pyrolysis deposition system. The idea is to generate droplets from a spray solution and send them, with some initial velocity, towards the substrate surface. Spray pyrolysis normally uses air blast, ultrasonic, or electrostatic techniques [27]. The atomizers differ in resulting droplet size, rate of atomization, and the initial velocity of the droplets. It has been shown that the size of the generated droplet is not related to any fluid property of the precursor solution and depends solely on the fluid charge density level ρ_e as shown in [28]

$$r^2 = \left(\frac{-\alpha'}{\beta'}\right)\frac{3\epsilon_0}{q\rho_e}, \tag{5}$$

where ϵ_0 is the permittivity, q is the elementary charge, and $-\alpha'/\beta'$ is a constant value equal to $\sim 1.0 \times 10^{-17}$ J. The mass of a droplet, assuming a spherical shape depends on its density

$$m = \frac{4\pi}{3}\rho_q r^3, \tag{6}$$

where r is the droplet radius and ρ_q is the droplet density. The initial leaving velocity of the droplet is an important parameter as it determines the rate at which the droplets reach the substrate surface, the heating rate of the droplet, and the amount of time the droplet remains in transport

Due to its ease of production, many companies chose to use pressure atomizers instead of the ultrasonic atomizers. Therefore, this work will mainly concern itself with the pressure and electrostatic atomizers, characterized in further detail in [17,27], respectively.

A pressure, or air blast, atomizer uses high speed air in order to generate an aerosol from a precursor solution. Increasing the air pressure causes a direct decrease in the generated mean droplet

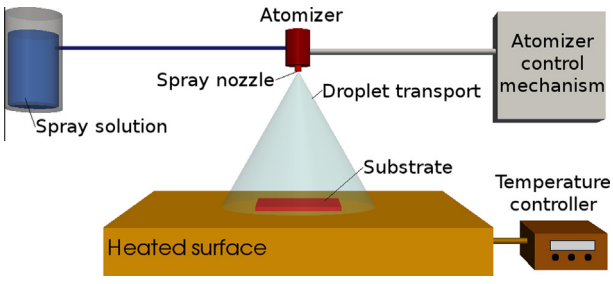

Fig. 2. General schematic of a spray pyrolysis deposition process.

diameter. Inversely, increasing the liquid pressure causes a direct increase in the mean droplet diameter [29]. Perednis [27] showed that all droplets sprayed from an air blast atomizer are contained within a 70° spray cone angle, while half are within a narrower 12° angle. It was also determined that the flow rate has a very small influence on the spray characteristics, which can be mostly ignored for modeling.

2.2. Aerosol transport of droplets

After the droplet leaves the atomizer, it travels through the ambient with an initial velocity determined by the atomizer. In the aerosol form, the droplets are transported with the aim of as many droplets as possible reaching the surface. As the droplets move through the ambient, they experience physical and chemical changes depicted in Fig. 3.

As the droplet traverses the ambient, there are four forces simultaneously acting on it, describing its path. Those forces are gravitational, electrical, thermophoretic, and the Stokes force. As shown in Fig. 3, the droplets experience evaporation during their flight, which affects the influence of the forces on their trajectory. Some experimental results from [30] indicate that solid particles could form, when the reactor temperature is low, when the precursor solution concentration is high, and when the flow rate of the carrier gas (N_2) is low.

2.2.1. Gravitational force

The gravitational force is the force pulling the droplet downward. The size of the force depends on the mass of the traveling droplet, given by Eq. (6). For small droplets the force of gravity is too small to allow it to arrive at the surface before it is fully evaporated. For larger particles, the force of gravity is the driving force behind the droplet transport.

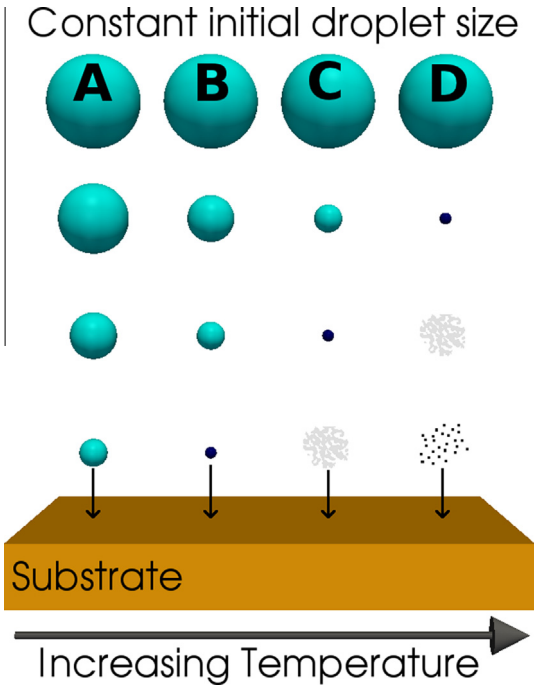

Fig. 3. Spray pyrolysis droplets modifying as they are transported from the atomizing nozzle to the substrate. Whether the temperature [31] or the initial droplet size [32] are varied, there are four potential paths which the droplet can take as it moves towards the substrate (A–D).

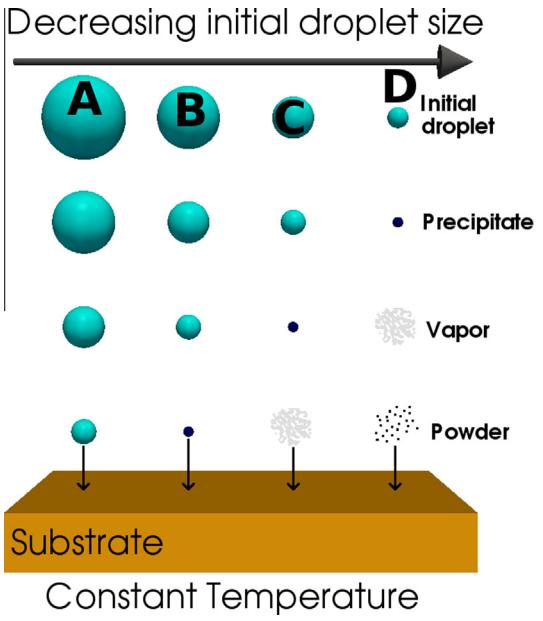

Fig. 3 (*continued*)

2.2.2. Electrical force

The electrical force is applicable to spray pyrolysis systems which include an additional electrical source governing the droplet's trajectory. When an air blast atomizer is used, high speed air is the cause of atomization and aerosol production. Ultrasonic atomizers are electrically driven, whereby an electric generator is vibrated at ultrasonic frequencies through a titanium nozzle. Increasing the frequency can result in smaller droplet sizes. Electric spray deposition (ESD) atomizers use a strong electric field at the liquid–gas interface to generate charged droplets. Therefore, air blast atomizers do not have additional contributions from an electrical force and the droplet transport is driven by the gravitational force and the initial velocity, while for spray pyrolysis deposition using ultrasonic and ESD atomizers, the electrical force is the main component which drives the droplets downwards. The electrical force acting on a droplet is usually several orders of magnitude larger than the gravitational force [15] and is given by

$$F_e = q_d E, \tag{7}$$

where E is the generated electric field strength and q_d is the droplet charge. q_d depends on the temporal change of the droplet and is given by

$$q_d = 8\pi\sqrt{\gamma\epsilon_0 r^3}\cdot\frac{t}{t+t_0}, \qquad t_0 = \frac{4}{b\,\mathrm{div}E} \tag{8}$$

where γ is the liquid–gas surface tension, ϵ_0 is the electrical permittivity, and b is the ionic mobility [32].

2.2.3. Stokes force

The stokes force is the drag experienced by the droplet due to the air resistance in the ambient. The force is caused by the friction between the droplet and air molecules. The Stokes force is a factor of the particle's velocity and size. Therefore, large droplets which move with a high velocity will experience the largest retarding force according to

$$F_S = 6\pi\eta_a r(v_d - v_a)\left(1+\frac{3}{8}\mathrm{Re}\right), \tag{9}$$

where η_a is the viscosity of air, v_d is the droplet velocity, v_a is the air velocity, and Re is the Reynolds number.

For spherical particles, the Reynolds number is given by

$$\mathrm{Re} = \frac{2r(v_d - v_a)\rho_a}{\eta_a}, \tag{10}$$

where ρ_a is the density of air. Because the 3/8 Re term in Eq. (9) is very small ($3/8\ \mathrm{Re} \ll 1$), it is often excluded from Stokes force calculations.

2.2.4. Thermophoretic force

The thermophoretic force is a retarding force, causing droplets to significantly decrease their velocity as they approach the heated substrate. Fig. 4 shows the temperature distribution near a heated substrate. The results for the 210 °C, 250 °C, and 310 °C samples are taken from [27], while the results for the 400 °C sample are measured. It is evident that the air temperature increases steeply due to the forced convection cooling effect of the air flow when close to the heated substrate. Because the thermophoretic force depends on the thermal gradient in the transport environment, it can be concluded that it will have no effect on the droplet movement, when it is more than several (~5–7) mm away from the substrate. However, in this high thermal gradient region, the thermophoretic force begins to dominate. This is true for pressure spray deposition (PSD) systems where the main driving force is gravity; however, for ESD systems, the electrical force is often stronger than the thermophoretic force [27]. The increased temperature has additional effects on the droplet, such as a reduction in its size due to droplet evaporation in the region.

The equation governing the strength of the thermophoretic force is given by

$$F_t = \frac{3\pi\eta_a^2 r}{\rho_a} \cdot \frac{3\kappa_a}{2\kappa_a^2 + \kappa_d} \cdot \frac{\nabla(T_a)}{T_a}, \tag{11}$$

where η_a is the viscosity of air, T_d is the droplet temperature, T_a is the air temperature, ρ_a is the density of the air, and κ_a and κ_d are the thermal conductivities of the air and the droplet, respectively. It should be mentioned that Eq. (11) is only valid for droplets whose radius is much larger than the mean free path of the air molecules.

2.3. Precursor decomposition

The precursor, as it moves through the heated ambient undergoes various changes, which are characterized in Fig. 3. Evaporation, precipitate formation, and vaporization all occur depending on the droplet size and ambient temperature. Fig. 3 shows the four physical forms in which the droplet may interact with the substrate surface. Although all processes occur during deposition, Process C, the CVD-like deposition is desired to yield a dense high quality film [27].

2.3.1. Process A: low temperature-large initial droplet

When the large droplets approach a heated substrate and the temperature is not sufficiently high to fully evaporate the solution, they will impact with the substrate and decompose. Upon contact, the droplet is entirely vaporized and a dry precipitate is left behind. Because droplet vaporization requires some heat, the substrate temperature is slightly decreased at the impact point, adversely affecting the reaction kinetics [32]. This process has a weak sticking probability.

2.3.2. Process B: low/intermediate temperature-large/medium droplet size

When medium-sized droplets are initially formed, some evaporation occurs. Just as the droplet reaches the surface, however, it forms a precipitate as an amorphous salt and a dry precipitate hits the surface, where decomposition occurs. Some particles evaporate and condense into gaps between particles, where surface reaction occurs. However, this process has a medium sticking probability.

2.3.3. Process C: intermediate/high temperature-medium/small droplet size

When the processing environment causes droplets to evaporate prior to reaching the substrate vicinity, a precipitate will form early. As the precipitate reaches the immediate vicinity of the substrate, it is converted into a vapor state and it undergoes a heterogeneous reaction through the following steps [32]:

1. Reactant molecules diffuse to the surface.
2. Adsorption of some molecules at the surface.
3. Surface diffusion and a chemical reaction, incorporating the reactant into the lattice.
4. Desorption and diffusion of the product molecules from the surface.

This is a classical CVD reaction, which results in a high quality film deposition and a high sticking probability.

2.3.4. Process D: high temperature-small droplet size

When small initial droplets are formed, or the temperature is high enough, the droplet quickly forms a precipitate. As the precipitate approaches the substrate, it is vaporized and a chemical reaction subsequently occurs in the vapor phase. This homoge-

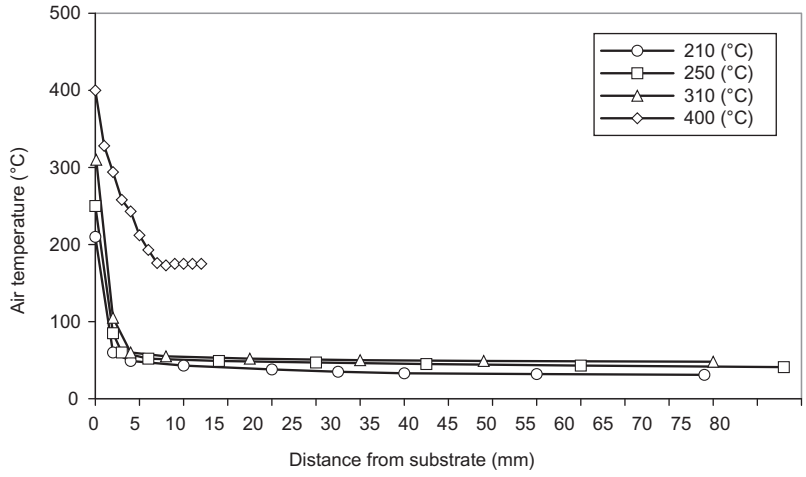

Fig. 4. Air temperature above a heated plate for substrate temperatures 210 °C, 250 °C, 310 °C, and 400 °C during a pressurized spray process.

neous reaction leads to the condensation of molecules into crystallites in the form of a powder precipitate. The powder falls to the substrate surface, but without a deposition reaction.

3. Modeling droplet transport

Forces acting on the droplet can be used in order to calculate the location where the droplet makes impact with the surface. This is a challenge because the simulation environment must now be divided into several segments. The first segment which must be treated separately is the thermal zone which is within 10 mm of the wafer surface. In this area, the temperature gradient shown in Fig. 4 is high and the thermal forces play a significant role in the droplet speed as well as size, due to evaporation. In addition, when the electrical force is included, the complexity of the problem is significantly increased.

Fig. 5 shows how the simulation space is divided in order to accommodate the thermal zone for droplets. A detailed derivation of the droplet transport equations can be found in [33].

3.1. Effects of external forces on droplet transport

In order to follow the trajectory of a droplet after leaving the atomizer and under the influence of gravity, Stokes, electric, and thermophoretic forces, the distance required for the droplet to travel, the initial velocity v_0, and the droplet radius r_d are known. Although the thermophoretic force does not affect the droplet motion until it reaches the vicinity of the wafer, it will be included in the derivation of the equations of motion. This allows for the most complex system to be solved, which includes all forces. Given the four forces discussed previously, the vertical acceleration experienced by the particle is given by

$$a_v(t) = g - l + s v_v(t) + c d_v(t), \tag{12}$$

where g and l are the accelerations caused by the gravitational and thermophoretic forces, respectively. Acceleration s is velocity-dependent and caused by the Stokes force, while c is the linearized displacement-dependent acceleration due to the electrical force

$$l = \frac{27\eta_a^2\kappa_a\nabla T}{4\rho_a\rho_d T(2\kappa_a+\kappa_d)r_d^2}, \qquad s = \frac{9\eta_a}{2\rho_d r_d^2},$$
$$c_v = \frac{6}{\rho_d}\sqrt{\frac{\gamma\epsilon_0}{r_d^3}}\cdot\frac{\Phi_0}{H}\cdot\frac{K_V}{\log(4H/R)}c_e, \tag{13}$$

where Φ_0 and H are the applied electrical potential and distance between the nozzle and substrate, respectively. R is the outer radius of the nozzle, while K_V is a value which ranges from 0 to 1 depending on the H/R ratio [34]. The variable c_e is a linearization constant which represents a best-fit to the electric field in the region. Fig. 6 shows the value for the normalized potential $\Phi^* = \Phi/\Phi_0$ and its distribution in an ESD deposition setup. The atomizing nozzle is located at $(0, 1)$. The inset shows the electric field distribution in the same simulation space. It is evident that the strength of the electric field is not uniform or linear, but that the field causes charged droplets to spread radially.

For the purposes of spray deposition, it is often assumed that the value of K_V is 1, because the ratio of H/R is on the order of several hundreds, which gives a value close to 1 for K_V. This value is adjusted in the model using the relationship

$$K_V = 1 - e^{-0.021\frac{H}{R}}. \tag{14}$$

In fact, assuming that $K_V = 1$ can cause erroneous results for the electric field. The negative exponential dependence on R from Eq. (14) is in the numerator of c_v in Eq. (13), which shows an additional inverse logarithmic dependence in the denominator. A plot of the fraction $K_V/[\log(4H/R)]$ for various R values is shown in Fig. 7, when the variation in K_V is taken into account and when it is assumed that $K_V = 1$. It is clear that the effects of K_V should be included in the droplet transport model when $R/H > 0.005$.

3.1.1. Vertical trajectory

The droplet displacement resulting from the acceleration given in Eq. (12) is given by

$$d_v(t) = C_1 e^{-r_1 t} + C_2 e^{-r_2 t} + C_3, \tag{15}$$

where

$$r_1 = \frac{-s+\sqrt{s^2-4c_v}}{2}, \quad r_2 = \frac{-s-\sqrt{s^2-4c_v}}{2}, \tag{16}$$

and

$$C_1 = r_1 v_{v0} - \frac{r_1^2 r_2}{r_1 - r_2}\left[(g-l) - v_{v0}\left(\frac{1}{r_1}+s\right)\right],$$
$$C_2 = \frac{r_1 r_2^2}{r_1 - r_2}\left[(g-l) - v_{v0}\left(\frac{1}{r_1}+s\right)\right],$$
$$C_3 = \frac{c_v}{1+(g-l)+s}. \tag{17}$$

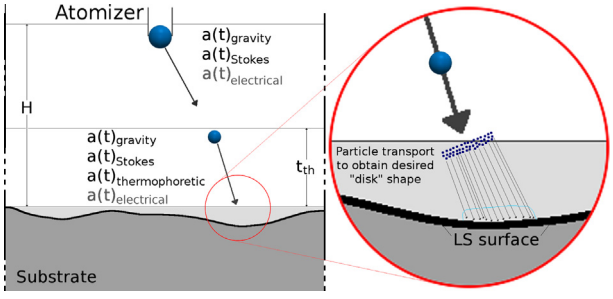

Fig. 5. The droplet transport in the space above the substrate surface and the accelerations which are considered in the transport model. T_{th} is the height of the thermal zone (~10 mm for ESD, ~5 mm for PSD), and H is the distance between the substrate and atomizer.

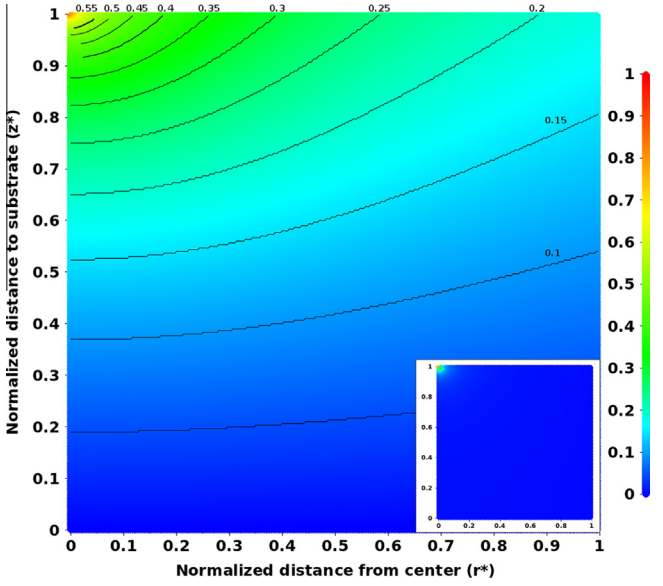

Fig. 6. Magnitude of the normalized electric potential Φ/Φ_0 during ESD processing. The distance between needle and deposition plate as well as the radial distance from the center are normalized to the distance between the atomizer and the substrate. The inset is the normalized electric field distribution.

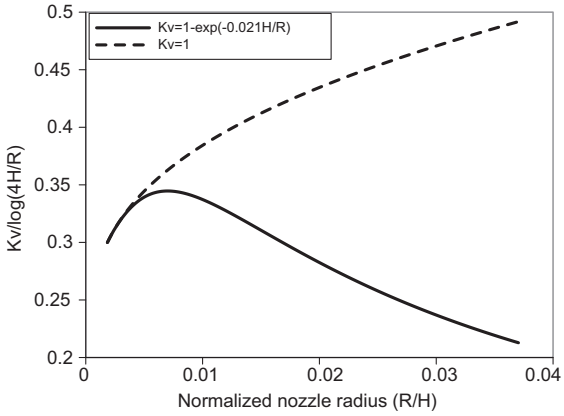

Fig. 7. The effects of varying the atomizing nozzle's outer radius on the strength of the electric field with and without the K_V effects.

It should be noted that, if the initial displacement is set to 0, then $A_1 = B_1 = 0$. Similarly, if the initial velocity is also set to 0, then $A_2 = B_2 = 0$, significantly reducing the complexity of the problem. Since the vertical displacement is a known value and is dependent on the placement of the atomizing tip above the wafer, it is more important to calculate the time t required for the droplet to traverse the vertical displacement in order to reach the wafer height. Attempts to invert Eq. (15) in order to obtain t fails to result in an explicit mathematical expression. This means that the time t must be solved using time discretization, Monte Carlo (MC) methods, or iteratively. An iterative solver is implemented within the presented simulator.

3.1.2. Radial trajectory

In order to calculate the radial trajectory, the time t from Eq. (15), radius r_d, and initial velocity v_{r0} must be known. These parameters are derived using the vertical trajectory discussion. Gravity and thermophoretic forces are vertical forces only and do not influence the radial movement of the droplet; therefore, only the Stokes force and the electrical forces must be considered. The acceleration of the droplet is defined by

$$a_r(t) = s v_r(t) + c_r d_r(t), \tag{18}$$

Similar methods as for the vertical trajectory can be used to solve the radial velocity and displacement. When the radial displacement is calculated, the location at which the droplet contacts the wafer is known and locallized deposition can proceed. The radial displacement is given by

$$d_r(t) = D_1 e^{-r_1 t} + D_2 e^{-r_2 t}, \tag{19}$$

where

$$r_1 = \frac{-s + \sqrt{s^2 - 4c_r}}{2}, \quad r_2 = \frac{-s - \sqrt{s^2 - 4c_r}}{2}, \tag{20}$$

and

$$D_1 = r_1 v_{r0} - \frac{r_1^2 r_2}{r_1 - r_2}\left[v_{r0}\left(\frac{1}{r_1} + s\right)\right], D_2 = \frac{r_1 r_2^2}{r_1 - r_2}\left[v_{r0}\left(\frac{1}{r_1} + s\right)\right]. \tag{21}$$

The location where the droplet contacts the wafer and where deposition proceeds is at a radial distance $d_r(t)$ away from the needle tip.

3.2. Droplet transport inside the heat zone

An additional effect which occurs in the heat zone is the significant increase in the mean droplet radius noticed in measurements [27]. The reason behind this increased mean radius is that droplets with a small radius evaporate before reaching the surface, while larger droplets, although also evaporating slightly, stay relatively complete until fully in contact with the surface. Tracking of the detailed changing droplet size during its travel through the heat zone does not modify the model enough to merit the additional computational expense. Therefore, the model automatically excludes droplets which are too small to influence deposition, while other droplets which reach the surface have their radius reduced as they enter the heat zone. The approximate relationship which governs the small droplet's lifetime is given by [35]

$$t_{life} = \frac{4 r_{init}^2}{q_0 \triangle T}, \tag{22}$$

where r_{init} is the initial droplet radius, q_0 is an evaporation rate constant, and $\triangle T$ is the temperature difference within the droplet. The exact solution for the decrease of the radius of a droplet requires the solution of a diffusion equation, since the evaporation of a droplet is given by [35]

$$\frac{dr_d}{dt} = \frac{-M_W D_{vf}}{r_d \rho_d R T_f} \triangle p\left(1 + 0.276 Re^{1/2} Sc^{1/3}\right), \tag{23}$$

where M_W is the molecular weight of the evaporating liquid, D_{vf} is the average diffusion coefficient for vapor molecules in the saturated film around the droplet at the final temperature T_f, R is the gas constant, $\triangle \rho$ is the pressure difference between the vapor pressure near the drop and the ambient pressure, and Re and Sc are the dimensionless Reynold's and Schmidt's numbers, respectively, given by

$$Re = \frac{2\rho_a v t r_d}{\eta_a}, \quad \text{and } Sc = \frac{\eta_a}{\rho_a D_{vf}}. \tag{24}$$

The average diffusion coefficient D_{vf} is estimated using the Stokes–Einstein relationship

$$D_{vf} = \frac{R T_f}{N_A} \frac{1}{6\pi \eta_d r_d}, \tag{25}$$

where N_A is Avogadro's number. The droplet radius r_d and velocity vt are time dependent; therefore, the change in radius through the heat zone can only be solved numerically using a time discretization technique. However, large droplets do not experience significant size reduction through a zone with a non-zero temperature gradient ΔT. Also, it can be assumed that a sedimentation velocity is reached relatively quickly and does not change with time. The diffusion of the droplet can be approximated linearly by

$$K = q_0 \triangle T (1 + 2 q_1 r_d), \tag{26}$$

where K represents the surface evaporation rate in (m^2/s) with $K = -\frac{dr_d^2}{dt}$, while q_0 and q_1 are given by

$$q_0 = \frac{2a}{\triangle T}(1 + b s_0), \qquad q_1 = \frac{b r_0}{1 + b s_0}, \tag{27}$$

where r_0 and s_0 are constants given by $r_0 = 64.65\ s^{-0.5}$ and $s_0 = -1.117 \times 10^{-3}\ ms^{-0.5}$ and the variables a and b are given by

$$a = \frac{4\gamma M_W D_{vf}}{\rho_d R} \frac{\triangle T}{T_f}, \qquad b = 0.276\left(\frac{\rho_a}{\eta_a D_{vf}^2}\right)^{1/6}, \tag{28}$$

where γ is a constant [35]. With the goal of a topographical simulation in mind, a full detailed analysis for the droplet size, as it changes in the heat zone is not merited. Therefore, in order for Eqs. (22)–(28) to be included in the model, some assumptions are made:

1. Droplets with a radius which is too small, giving a small t_{life} will not be taken into account, since those droplets will never reach the surface.
2. While the droplet is traveling through the heat zone, the forces acting on it do not change. Rather, the effects of the heat is represented by a single reduction in droplet radius, which is calculated following the above discussion.
3. The velocity of the droplet through the heat zone is assumed to be constant in order for the above analysis to be valid and to calculate the size reduction due to thermal effects. The change in velocity from the time when the droplet enters the heat zone until it reaches the surface will, nevertheless, be calculated using the forces at play and the modified droplet size from Eqs. (22)–(28).

3.3. Modeling interaction between droplet and wafer surface

There are two main types of depositions which have been examined. One type relies on the droplets being transported very near the surface, where they undergo evaporation and the resulting vapor causes a CVD-like deposition process on the silicon surface. The other type relies on the droplet reaching the surface before it is fully evaporated and sticking on the silicon wafer while simultaneously spreading. The former is commonly the result of a PSD deposition process, while the latter is common for ESD processes, where the droplets are accelerated at much higher speeds and therefore have enough force to overcome the retardant Stokes and thermophoretic forces to reach the substrate as a liquid.

4. Spray pyrolysis deposition simulations

4.1. YSZ deposition using ESD pyrolysis

The YSZ deposition using an ESD process from [27] is simulated using the model discussed in the previous section. The first step is finding the droplet size as it exits the atomizer. The distribution of droplet sizes does not follow any standard distribution, but it is suggested that the volume fraction varies relatively evenly near the approximate value 0.05 for droplets with a radius between 2.5 μm and 55 μm [27,36]. Therefore, the distribution for the droplet radii is simulated by generating an even distribution for the volume fraction ξ_{vol} followed by finding the radius distribution for the droplet r_d:

$$r_d = \left\{ \xi \cdot \left[(r_+)^{-1/3} - (r_-)^{-1/3} \right] + (r_-)^{-1/3} \right\}^{-3}, \tag{29}$$

where $r_- = 2.5\,\mu m$ and $r_+ = 55\,\mu m$ are the minimum and maximum radii for the generated droplets and $\xi \in [0, 1]$ is an evenly distributed random value.

The given equation for the electric field provides the magnitude at each location; however, in order to follow the droplet trajectory, the individual components of the electric field in each direction are required such that, in cylindrical coordinates, $\vec{E}_{ext} = (E_\rho, \varphi, E_z)$. The droplet angle φ is unaffected by the applied forces since they act only in the radial ρ and vertical z directions.

Fig. 8 shows a silicon surface geometry which extends 50 mm by 50 mm after 1, 10, 20, 50, and 100 spray cycles with 100,000 droplets per cycle and the spray nozzle located 270 mm above the surface. Few details are visible and visualizing the film growth as droplets interact with the wafer surface is only possible, when a smaller surface area is examined.

Fig. 9 shows an area which expands 250 μm by 250 μm. Several droplets are shown including overlapping of the disk shapes on the surface as they are being deposited. The lighter surface is silicon while the darker disks are the deposited YSZ films. Each depositing droplet is modeled using 10^9 particles which accelerate to the surface and add a slight component of the overall deposited film thickness.

4.2. Tin oxide deposition using PSD pyrolysis

The deposition of tin oxide (SnO_2) on silicon dioxide using the spray pyrolysis deposition process was performed using an air atomizer which is not located directly above the wafer, but rather on the side, emitting a spray towards the wafer. The nitrogen pressure of the atomizer was set to 2 bar in air and 0.7 bar in the liquid. These values are outside of the data sheet for the nozzle used [29], which is done in order to obtain smaller droplet sizes and slower deposition rates [3]. However, the data sheet information was extracted and the provided graph extended in order to find an approximate radial distribution of particles. The droplet radii vary between 1.5 μm and 5.5 μm. The spray direction is also extrapolated from the data sheet for the simulation. The spray nozzle in use is one which produces a flat spray pattern with droplet dispersal proceeding mainly in the lateral axial direction. The nozzle is approximately 20 cm laterally and 10 cm vertically distanced from the substrate and the spray is directed such that much of it is found above the heated surface, where it can deposit onto the wafer.

In the ESD system, the flight of individual droplets was modeled in order to analyze the film deposition. However, in the PSD system, due to the lack of a strong electrical force, it is clear that the droplets cannot be viewed individually, but that interactions between droplets during their flight plays a significant role in their trajectory. Droplets move through air as a flux and calculating individual droplet's movements in order to find their final location on the wafer surface does not produce a match to the experimental results, shown in Fig. 10(a).

There are several factors which influence the final thickness of the deposited film. Those include the spraying time, volume of the sprayed solution, air pressure, distance of the atomizer from the substrate, temperature of the pyrolysis reaction, and time of the solution ($SnCl_4$) aging. It was found in [17] that thicknesses of the deposited SnO_2 film decrease, when the time interval be-

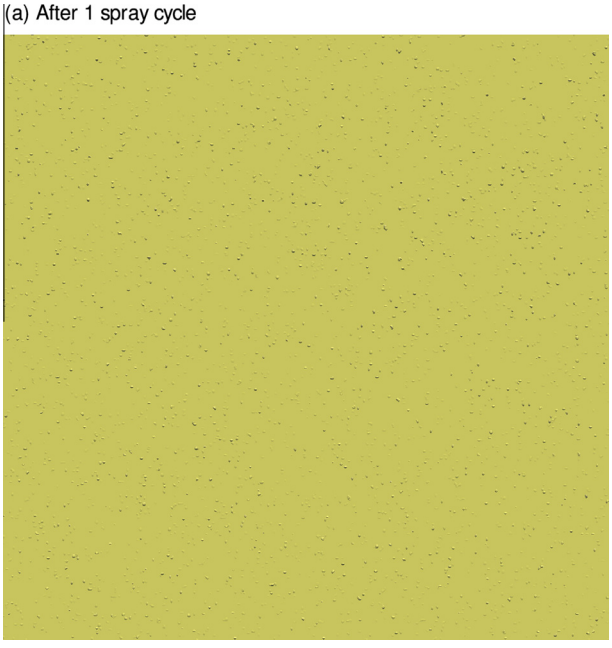

Fig. 8. Macroscopic spray pyrolysis simulation on a 50 mm by 50 mm geometry. Each spray cycle contains 100,000 droplets. (a) After 1 spray cycle; (b) after 20 spray cycles; (c) after 50 spray cycles; (d) after 100 spray cycles.

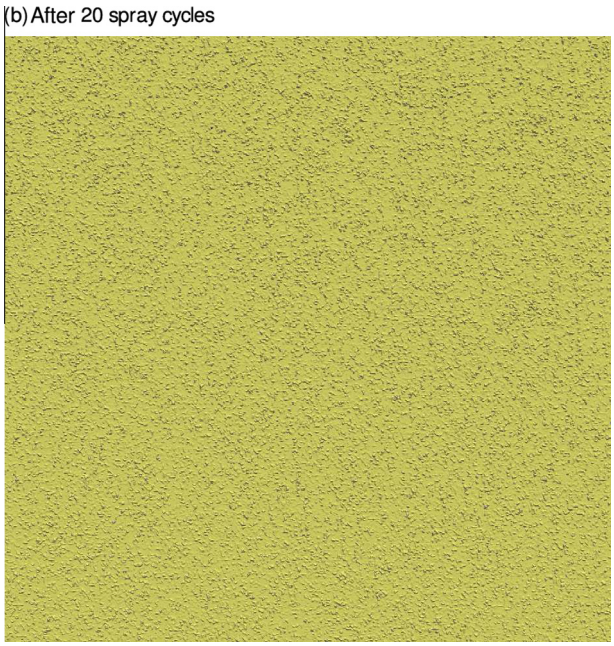

Fig. 8 (*continued*)

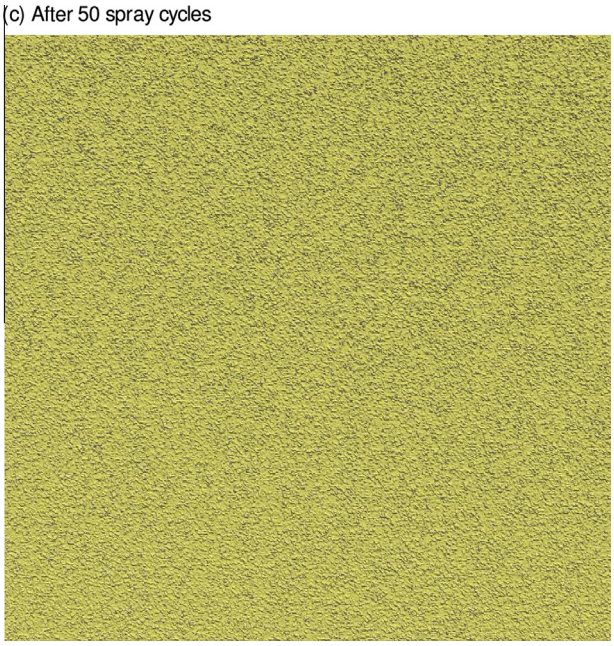

Fig. 8 (*continued*)

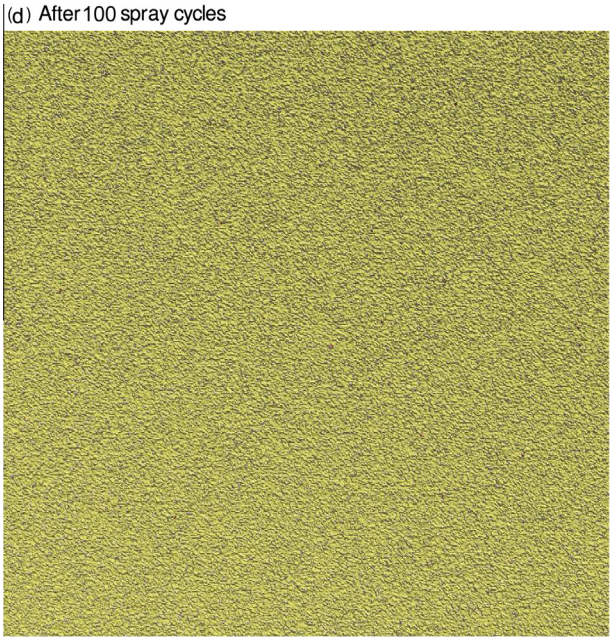

Fig. 8 (*continued*)

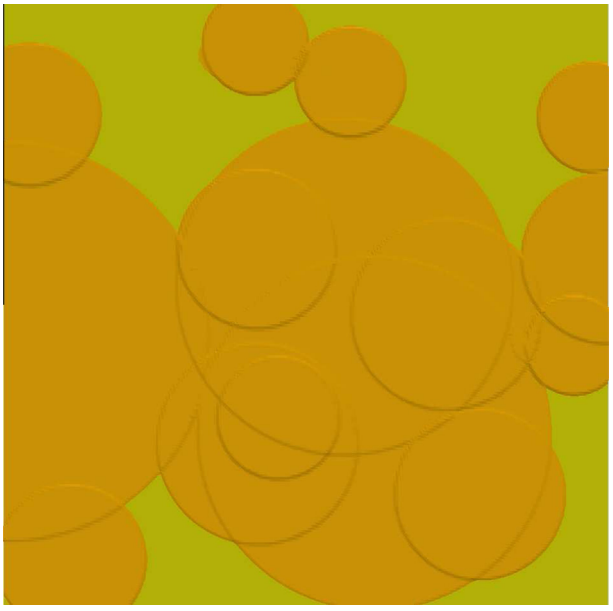

Fig. 9. caption - Spray pyrolysis simulation on a 250 μm by 250 μm geometry. (a) 15 droplets; (b) 100 droplets.

tween its preparation and its use in the pyrolysis reaction increases. A suggestion is made to use either a freshly made solution or a completely aged solution during spray pyrolysis. During the presented experiments, the nozzle distance to the substrate, air pressure, and solution aging remain constant, while the spray is constantly applied. The nozzle's distance to the substrate is set to 20 cm laterally and 10 cm vertically, the air pressure to 1 atm, and the solution is freshly prepared. In correspondence, the time and temperature dependences are investigated in the model.

Our experimental data suggest a linear dependence on spray time and a logarithmic dependence on wafer temperature for the growth rate of the deposited SnO_2 layer. A good agreement is given by the Arrhenius expression

$$d_{SnO_2}(t,T) = A_1 t e^{(-E/k_B T)}, \tag{30}$$

where $A_1 = 3.1$ μm/s, the thickness is given in μm, t is the time in seconds, T is the temperature in Kelvin, and E is 0.427 eV. Fig. 10 depicts the (a) experimental and (b) simulated topography of a deposited SnO_2 film on a step structure after applying a PSD process for 45 s at 400 °C. The incoming flux is set to flow in the $(x,y) = (-0.32,-0.95)$ direction and a CVD-like process is simulated with a reaction order of 1 and a sticking probability of 0.2, producing a good fit to the experimental data. The average direction of the initial flow is $(-1,0)$, but due to the effects of gravity in the vertical direction, the droplet flux experiences a downward acceleration. However, in the lateral motion, it only experiences the retardant

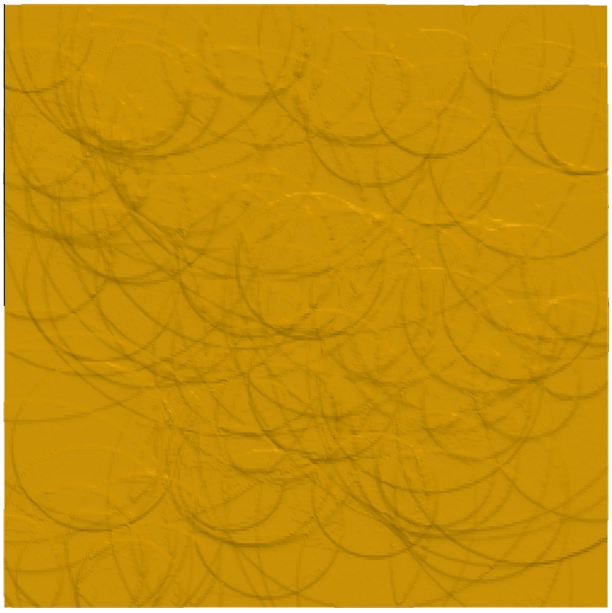

Fig. 9 (*continued*)

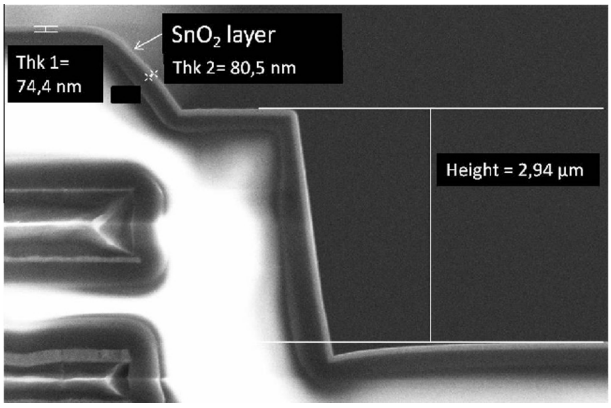

Fig. 10. Images showing the deposited SnO_2 film as a results of a PSD deposition step. The good step coverage confirms a chemical and not physical reaction takes place during deposition. (a) SEM image; (b) simulation.

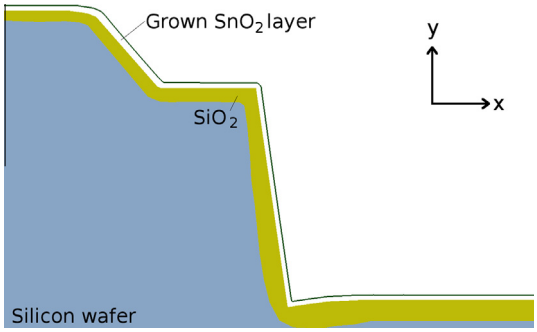

Fig. 10 (*continued*)

Stokes force. Therefore, it is evident that the direction of the flux will change from mainly horizontal to mainly vertical as it reaches the wafer.

5. Conclusion

In order to manufacture smart gas sensor devices, the spray pyrolysis deposition technique is used to grow an ultrathin SnO_2 layer. The thin film reacts with the gas at high temperatures to allow for charge transfer between the gas and surface, modifying the electrical conductance in the process. The spray pyrolysis technique is found to be cost effective and is implementable as post-CMOS backend process. A model for spray pyrolysis deposition has been presented and integrated into a topography process simulator using the Level Set method. The model examines two possible interactions between droplets and the semiconductor wafer surface. The first, using an electrical nozzle, calculates the trajectories of all generated droplets and each droplet's point of impact at the wafer surface determines a deposition disk. Very small droplets, which evaporate prior to reaching the wafer's vicinity are excluded from the simulation, while the remaining droplets combine to form the final deposited thin film. However, it was observed that, when a pressure nozzle is used, and a strong electric field is not present to govern the droplet trajectories, a deposition model similar to CVD is more appropriate. Therefore, the second model viewes the droplet transport as a flux and not as individual particles. The droplets' evaporation near the heated wafer surface causes a vapor to form, which then deposits on the surface.

Acknowledgments

This work has been partly performed in the COCOA-CATRENE European project and in the project ESiP. In this latter the Austrian partners are funded by the national funding institution for applied research and development in Austria, the Austrian Research Promotion Agency (FFG) under Project No. 824954 and the ENIAC Joint Undertaking. The work has also been partly performed in the Christian Doppler Laboratory for Reliability Issues in Microelectronics at the Institute for Microelectronic.

References

[1] W. Göpel, K. Schierbaum, Sens. Actuators B: Chem. 26–27 (1995) 1–12.
[2] J. Kappler, A. Tomescu, N. Barsan, U. Weimar, Thin Solid Films 391 (2001) 186–191.
[3] A. Tischner, T. Maier, C. Stepper, A. Köck, Sens. Actuators B: Chem. 134 (2) (2008) 796–802.
[4] A. Tischner, A. Köck, Spray pyrolysis for the fabrication of tin dioxide nanostructures for gas sensing applications, in: Pyrolysis: Types, Processes, and Industrial Sources and Products, Nova Science Publishers, New York, 2009.
[5] E. Brunet, T. Maier, G. Mutinati, S. Steinhauer, A. Köck, C. Gspan, W. Grogger, Sens. Actuators B: Chem. 165 (2012) 110–118.
[6] J. Mochel, US Patent 2,564,707.
[7] J. Hill, R. Chamberlin, US Patent 3,184,084.
[8] G. Mutinati, E. Brunet, S. Steinhauer, A. Köck, J. Teva, J. Kraft, J. Siegert, F. Schrank, E. Bertagnolli, Proc. Eng. 47 (2012) 490–493.
[9] C. Griessler, E. Brunet, T. Maier, S. Steinhauer, A. Köck, J. Teva, F. Schrank, M. Schrems, Microelectron. Eng. 88 (2011) 1779–1781.
[10] O. Ertl, Numerical methods for topography simulation, Dissertation, Technischen Universität Wien, Fakultät für Elektrotechnik und Informationstechnik, 2010.
[11] W.H. Press, Numerical Recipes: The Art of Scientific Computing, third ed., Cambridge University Press, 2007.
[12] B. Engquist, S. Osher, Math. Comput. 34 (149) (1980) 45–75.
[13] J.A. Sethian, Level Set Methods and Fast Marching Methods, second ed., Cambridge University Press, 1999.
[14] A. Nakaruk, C. Sorrell, J. Coat. Technol. Res. 7 (5) (2010) 665–676.
[15] D. Perednis, L.J. Gauckler, Solid State Ionics 166 (3–4) (2004) 229–239.
[16] R.R. Chamberlin, J.S. Skarman, J. Electrochem. Soc. 113 (1) (1966) 86–89.
[17] G. Korotcenkov, V. Brinzari, J. Schwank, M. DiBattista, A. Vasiliev, Sens. Actuators B: Chem. 77 (1–2) (2001) 244–252.
[18] S. Rozati, T. Ganj, Renew. Energy 29 (10) (2004) 1671–1676.
[19] J. Manifacier, J. Fillard, J. Bind, Thin Solid Films 77 (1–3) (1981) 67–80.
[20] H. Koo, S. Hong, S. Ju, I. Seo, Y. Kang, J. Non-Cryst. Solids 352 (30–31) (2006) 3270–3274.
[21] F. Paraguay D., W. Estrada L., D.R. Acosta N., E. Andrade, M. Miki-Yoshida, Thin Solid Films 350 (1–2) (1999) 192–202.
[22] G.L. Messing, S.-C. Zhang, G.V. Jayanthi, J. Am. Ceram. Soc. 76 (11) (1993) 2707–2726.
[23] J.B. Mooney, S.B. Radding, Annu. Rev. Mater. Sci. 12 (1) (1982) 81–101.
[24] S. Major, A. Banerjee, K. Chopra, Thin Solid Films 108 (3) (1983) 333–340.
[25] S.H. Ng, J. Wang, D. Wexler, S.Y. Chew, H.K. Liu, J. Phys. Chem. C 111 (29) (2007) 11131–11138.
[26] G. Blandenet, M. Court, Y. Lagarde, Thin Solid Films 77 (1–3) (1981) 81–90.

[27] D. Perednis, Thin Film Deposition by Spray Pyrolysis and the Application in Solid Oxide Fuel Cells (Dissertation), Swiss Federal Institute of Technology Zurich, 2003.
[28] A.J. Kelly, Aerosol Sci. Technol. 12 (3) (1990) 526–537.
[29] Spraying Systems Co., Volume median diameter versus air pressure at constant liquid pressures, Data Sheet No. 36892-8M.
[30] I.W. Lenggoro, J. Mater. Res. 15 (3) (2000) 733–743.
[31] J.C. Viguié, J. Spitz, J. Electrochem. Soc. 122 (1975) 585–588.
[32] W. Siefert, Thin Solid Films 120 (4) (1984) 275–282.
[33] L. Filipovic, Topography Simulation of Novel Processing Techniques (Dissertation), Technischen Universität Wien, Fakultät für Elektrotechnik und Informationstechnik, 2012.
[34] A. Gañán-Calvo, J. Lasheras, J. Dávila, A. Barrero, J. Aerosol Sci. 25 (6) (1994) 1121–1142.
[35] H. Holterman, Kinetics and Evaporation of Water Drops in Air, IMAG, Wageningen, Netherlands, 2003.
[36] O. Wilhelm, Electrohydrodynamic Spraying – Transport, Mass and Heat Transfer of Charged Droplets and Their Application to the Deposition of Thin Functional Films (Dissertation), Swiss Federal Institute of Technology Zurich, 2004.